STATOR CURRENT ANALYSIS OF INCIPIENT FAULT INTO ASYNCHRONOUS MOTOR ROTOR BARS USING FOURIER FAST TRANSFORM

Arezki Menacer [*]**— Mohamed-Saïd Naît-Saïd** [**]
A/Hamid Benakcha [*]**— Saïd Drid** [**]

Recently, research has picked up a fervent place in the area of fault diagnosis of electrical machines. Like adjustable speed drives, fault prognosis has become almost indispensable. Motor current signature analysis is a condition monitoring technique that is now widely used to diagnose problems such as rotor bars broken, abnormal levels of air gap eccentricity, shorted turns in low voltage stator windings, and some mechanical problems.

This paper presents the effect of the broken bar time evolution since the created incipient fault on the various characteristics of the induction machine such as torque, speed and current. This one is simulated while the rotor bar resistance may be varied linearly versus time since its normal value to the final broken bar situation (partial to total broken bar). In this way we can observe the incipient fault impact on the different characteristics of the machine quantities (torque, speed and current).

K e y w o r d s: fault simulation, mathematical models, condition monitoring, asynchronous (induction) motors, incipient broken bar, resistance bar, resistance time ratio

1 INTRODUCTION

The problem of diagnosis is indeed related to that of the maintenance, utilizing economic factors that are difficult to evaluate. The issues of preventive and condition-based maintenance, online monitoring, system fault detection, diagnosis, and prognosis are of increasing importance.

The key issues for a successful motor operation are a quality motor, understanding its application, choice of the proper one for the application, and its proper maintenance. The use of induction motors in today's industry is extensive and they can be exposed to different hostile environments, manufacturing defects, *etc* [1].

The problem of the broken bars in the induction motors of offshore oilrig pumping stations, which were the first research tasks of diagnosis, is a good example [2]. Several works followed in the same way [3-6], or initiated in the diagnosis of other failures of the machine like the eccentricity of the rotor [7], the open circuits [8], [9], [5], the wear of the stages [10], [11]. These types of faults usually refer to the gradual deterioration of the motor that can lead to motor failure if undetected [1]. Monitoring of the current per phase can provide indications on the motors state. This is preferable, compared to other methods since it is easy for physical measurement. The fault affects the spectrum current signal while the induction machine is sufficiently loaded and generally we can extract from that the number of the broken bars [6].

The motor current based fault detection relies on interpretation of the frequency components in the current spectrum that are related to rotor asymmetries. In order to study the phenomena taking place in the rotor, we model it in the form of NR mesh as shown in Fig. 1 [14].

2 INDUCTANCES IN INDUCTION MOTORS

The model assumptions are:
- negligible saturation and skin effect,
- uniform air-gap,
- sinusoidal mmf of stator windings in air-gap,
- rotor bars are insulated from the rotor, thus no inter-bar current flows through the laminations,
- relative permeability of machine armatures is assumed infinite.

Although a sinusoidal mmf of the stator winding is assumed, other winding distributions could also be analyzed by simply using superposition. This is justified by the fact that different space harmonic components do not interact [12].

To study the performance of squirrel cage induction motors with rotor fault, a mesh model of the rotor is selected as illustrated in Fig. 1 [12]. The development of the induction machine model has taken into account the effective geometry of the rotor that considers the rotor squirrel cage as a system of $(N_R + 1)$ identical and equally spaced loops. These inductances are conveniently

[*] Laboratory LGEB Department of Electrical Engineering 07000 Biskra University, Algeria, Menacer_arezki@hotmail.com, benakcha_a@yahoo.fr

[**] Laboratory LSPIE Propulsion-Induction Electromagnetic Electrical Engineering Department — University of Batna Rue Chahid Boukhlouf Med El Hadi 05000 Batna, Algeria, ms.naitsaid.@Lycos.com, s_drid@lycos.com
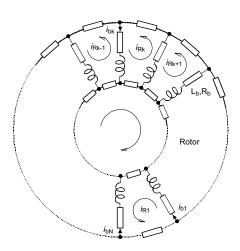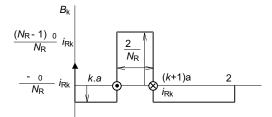
Fig. 1. Rotor cage equivalent circuit

Fig. 2. Form of magnetic induction of rotor mesh created by two bars

computed by means of an analytical approach. Generally this approach is based on a linear flux current relation.

A. Stator inductances

The expression of mmf of a phase is given by the following relation [13].

$$F_n(\theta) = \frac{2N_S i_{Sn}}{\pi p} \cos\left(\theta p - \frac{2\pi(n-1)}{3}\right). \tag{1}$$

By means of the above mentioned assumption the fundamental of the radial flux density in the air-gap can be written as:

$$B_{Sn} = \frac{2\mu_0 N_S}{\pi \delta p} i_{Sn} \cos\left(\theta p - \frac{2\pi(n-1)}{3}\right). \tag{2}$$

The main flux is thus written as:

$$\Phi_{Spn} = \frac{4\mu_0 N_S^2}{\pi \delta p^2}\left(\frac{D}{2}\right) l\, i_{Sn}. \tag{3}$$

The principal inductance of the magnetizing stator phase is:

$$L_{Sp} = \frac{\Phi_{Spn}}{i_{Sn}} = \frac{4\mu_0 N_S^2}{\pi \delta p^2}\left(\frac{D}{2}\right) l. \tag{4}$$

Therefore the total inductance of a phase is equal to the sum of the magnetizing and leakage inductances, thus:

$$L_S = L_{Sp} + L_{Sf}. \tag{5}$$

The mutual inductance between the stator phases is computed as:

$$M_S = -\frac{L_{Sp}}{2}. \tag{6}$$

B. Rotor inductance

The form of the magnetic induction produced by a rotor mesh in the air-gap is supposed to be radial and is represented in Fig. 2.

The principal inductance of a rotor mesh can be calculated from the magnetic induction distribution shown in Fig. 2 [13]:

$$L_{Rp} = \frac{2\pi\mu_0(N_R - 1)}{\delta N_R^2}\left(\frac{D}{2}\right) l. \tag{7}$$

The self and mutual rotor loops are obtained by considering each rotor loop k as an elementary mesh with a loop current i_{Rk}.

The total inductance of the kth rotor mesh is equal to the sum of its principal inductance, inductance of leakage of the two bars and inductance of the leakage of the two portions of rings of the short circuit closing the mesh k as indicated in Fig. 3.
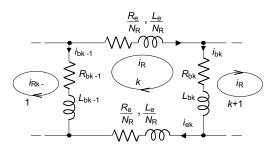

Fig. 3. Electric diagram equivalent of a rotor mesh

$$L_{RR} = L_{Rp} + 2L_b + 2L_e. \tag{8}$$

The mutual inductance between nonadjacent rotor meshes is expressed by the following relation deduced from Fig. 3

$$M_{RR} = -\frac{2\pi\mu_0 l}{\delta N_R^2}\left(\frac{D}{2}\right). \tag{9}$$

The kth mutual inductance between the adjacent meshes is given by:

$$M_{R_{k(k-1)}} = M_{R_{k(k+1)}} = M_{RR} - L_b. \tag{10}$$

In the same manner, the stator rotor mutual between the stator phase "1" and the kth rotor loop can be calculated using the flux linked to the rotor loop and is given by:

$$M_{Rk\,S1n} = -M_{SR} \cos\left(\theta - \frac{2\pi(n-1)}{3} + ka\right) \tag{11}$$

where:

$$a = \frac{2\pi}{N_R} p \quad \text{and} \quad M_{SR} = \frac{4\mu_0 N_S}{\pi \delta p^2}\left(\frac{D}{2}\right) l \sin\frac{a}{2}.$$

3 SQUIRREL CAGE INDUCTION MOTOR ROTOR MESH MODELLING

The mathematical model of squirrel cage induction motor can be written as:

$$[V] = [R][I] + \frac{\mathrm{d}}{\mathrm{d}t}([L][I]) \qquad (12)$$

where:

$$[V] = \begin{bmatrix} [V_S] \\ \cdots \\ [V_R] \end{bmatrix}, \quad [I] = \begin{bmatrix} [I_S] \\ \cdots \\ [I_R] \end{bmatrix}$$

with:

$$[V_S] = [V_S \quad V_S \quad V_S]^\top,$$
$$[V_R] = [0 \quad 0 \quad 0 \quad \cdots \quad 0]_{1 \times N_R+1},$$
$$[I_S] = [I_{S1} \quad I_{S2} \quad i_{S3}]^\top$$
$$[I_R] = [I_{R1} \quad I_{R2} \quad \cdots \quad I_{Rk} \quad \cdots \quad I_{RN_R} \quad I_e]^\top$$

The global resistance matrix can be written as:

$$[R] = \begin{bmatrix} [R_S]_{3\times3} & \vdots & [0]_{3\times N_R} & \vdots & [0]_{3\times1} \\ \cdots\cdots\cdots\cdots\cdots\cdots\cdots\cdots\cdots\cdots \\ [0]_{N_R\times3} & \vdots & [R_R]_{N_R\times N_R} & \vdots & -\frac{R_e}{N_R}[1]_{N_R\times1} \\ \cdots\cdots\cdots\cdots\cdots\cdots\cdots\cdots\cdots\cdots \\ [0]_{1\times3} & \vdots & -\frac{R_e}{N_R}[1]_{1\times N_R} & \vdots & R_e \end{bmatrix} \quad (13)$$

where:

$$[R_S]_{3\times3} = \begin{bmatrix} R_S & 0 & 0 \\ 0 & R_S & 0 \\ 0 & 0 & R_S \end{bmatrix}$$

and

$$[R_R]_{N_R\times N_R} =$$
$$\begin{bmatrix} R_{b0} + R_{b(N_R-1)} + 2\frac{R_e}{N_R} - R_{b0} & 0 & \cdots\cdots\cdots - R_{b(N_R-1)} \\ 0 & \cdots - R_{b(k-1)} \; R_{bk} + R_{b(k-1)} + 2\frac{R_e}{N_R} - R_{bk} & 0 & \ldots 0 \\ -R_{b(N_R-1)} & 0 \ldots 0 - R_{b(N_R-2)} \; R_{b(N_R-1)} + R_{b(N_R-1)} + 2\frac{R_e}{N_R} \end{bmatrix}$$

The complete matrix inductance can be represented by:

$$[L] = \begin{bmatrix} [L_S]_{3\times3} & \vdots & [M_{SR}]_{3\times N_R} & \vdots & [0]_{3\times1} \\ \cdots\cdots\cdots\cdots\cdots\cdots\cdots\cdots\cdots\cdots \\ [M_{RS}]_{N_R\times3} & \vdots & [L_R]_{N_R\times N_R} & \vdots & -\frac{L_e}{N_R}[1]_{N_R\times1} \\ \cdots\cdots\cdots\cdots\cdots\cdots\cdots\cdots\cdots\cdots \\ [0]_{1\times3} & \vdots & -\frac{L_e}{N_R}[1]_{1\times N_R} & \vdots & L_e \end{bmatrix}$$

where:

$$[L_S]_{3\times3} = \begin{bmatrix} L_{Sp} & M_S & M_S \\ M_S & L_{Sp} & M_S \\ M_S & M_S & L_{Sp} \end{bmatrix},$$

$$[M_{SR}]_{N_R\times3} = \begin{bmatrix} \cdots & -M_{SR}\cos(\theta + ka) & \cdots \\ \cdots & -M_{SR}\cos(\theta + ka - \frac{2\pi}{3}) & \cdots \\ \cdots & -M_{SR}\cos(\theta + ka - \frac{4\pi}{3}) & \cdots \end{bmatrix}$$

and

$$[L_R] =$$
$$\begin{bmatrix} L_{Rp} + 2L_b + 2\frac{L_e}{N_R} & M_{RR} - L_b & M_{RR} \\ M_{RR} - L_b & L_{R_p} + 2L_b + 2\frac{L_e}{N_R} & M_{RR} - L_b \\ M_{RR} & M_{RR} - L_b & L_{R_p} + 2L_b + 2\frac{L_e}{N_R} \\ M_{RR} & \vdots & \ddots \\ \vdots & \ddots & \ddots \\ M_{RR} - L_b & M_{RR} & M_{RR} \end{bmatrix}$$
$$\begin{matrix} M_{RR} & \cdots & M_{RR} - L_b \\ M_{RR} & M_{RR} & \cdots \\ M_{RR} - L_b & M_{RR} & \cdots \\ \ddots & \ddots & \ddots \\ \ddots & \ddots & \ddots \\ \cdots & M_{RR} - L_b \; L_{R_p} + 2L_b + 2\frac{L_e}{N_R} \end{matrix}$$

Using Park's transformation matrix in the stator, equation (12) can be written as:

$$[V_T] = [R_G][I_T] + \frac{\mathrm{d}}{\mathrm{d}t}([L_G][I_T]) \qquad (15)$$

where:

$$[V_T] = [V_{0S} \quad V_{dS} \quad V_{qS} \quad 0 \quad 0 \quad \ldots \quad 0 \quad \ldots \quad 0]^\top_{1\times N_R+4}$$
$$[I_T] = [I_{0S} \quad I_{dS} \quad I_{qS} \quad I_{R1} \quad I_{R2} \quad \ldots \quad I_{Rk} \quad \ldots \quad I_e]^\top_{1\times N_R+4}$$

Fig. 4. Variation order of resistance broken bar No 2

$[R_G] =$

$$
\begin{bmatrix}
R_S & 0 & 0 & \vdots \\
0 & R_S & 0 & \vdots \\
0 & 0 & R_S & \vdots \\
\cdots & \cdots & \cdots & \vdots \\
0 & 0 & T_1 & \vdots \\
0 & -T_1\sin(a) & T_1\cos(a) & \vdots \\
\vdots & \vdots & \vdots & \vdots \\
\vdots & \vdots & \vdots & \vdots \\
0 & -T_1\sin(N_R-1)a & T_1\cos(N_R-1)a & \vdots \\
\vdots & \cdots & \cdots & \vdots \\
0 & 0 & 0 & \vdots
\end{bmatrix}
$$

$$
\begin{array}{ccc}
0 & 0 & \cdots \\
0 & -T_1\sin(a) & \cdots \\
T_1 & T_1\cos(a) & \cdots \\
\cdots & \cdots & \\
R_{b0}+R_{b(N_R-1)}+2\frac{R_e}{N_R} & -R_{b0} & 0 \\
\ddots & \ddots & \ddots \\
0 & -R_{b(k-1)} & R_{b_k}+R_{b(k-1)}+2\frac{R_e}{N_R} \\
\ddots & \ddots & \ddots \\
-R_{b(N_R-1)} & 0 & \cdots \\
\cdots & \cdots & \cdots \\
-\frac{R_e}{N_R} & \cdots & \cdots
\end{array}
$$

$$
\begin{array}{ccc}
\cdots & 0 & \vdots \; 0 \\
\cdots & -T_1\sin(N_R-1)a & \vdots \; 0 \\
\cdots & T_1\cos(N_R-1)a & \vdots \; 0 \\
\cdots & \cdots & \vdots \; \cdots \\
\cdots & -R_{b(N_R-1)} & \vdots \; -\frac{R_e}{N_R} \\
\ddots & \ddots & \vdots \\
-R_{b_k} & 0 & \vdots \\
-R_{b(N_R-2)} & R_{b(N_R-1)}+R_{b(N_R-2)}+2\frac{R_e}{N_R} & \vdots \; -\frac{R_e}{N_R} \\
\cdots & \cdots & \vdots \; \cdots \\
\cdots & -\frac{R_e}{N_R} & \vdots \; R_e
\end{array}
$$

$[L_G] =$

$$
\begin{bmatrix}
L_S+2M_S & 0 & 0 & \vdots & 0 \\
0 & L_S-M_S & 0 & \vdots & L_{PR} \\
0 & 0 & L_S-M_S & \vdots & 0 \\
\cdots & \cdots & \cdots & \vdots & \cdots \\
0 & L_{PR} & 0 & \vdots & L_P \\
0 & L_{PR}\cos(a) & L_{PR}\sin(a) & \vdots & \ddots \\
\vdots & \vdots & \vdots & \vdots & M_{RR} \\
\vdots & \vdots & \vdots & \vdots & \ddots \\
0 & L_{PR}\cos(N_R-1)a & L_{PR}\sin(N_R-1)a & \vdots & M_{RR}-L_b \\
\cdots & \cdots & \cdots & \cdots & \cdots \\
0 & 0 & 0 & \vdots & -L_e/N_R
\end{bmatrix}
$$

$$
\begin{array}{ccccc}
0 & \cdots & \cdots & 0 & \vdots \; 0 \\
L_{PR}\cos(a) & \cdots & \cdots & L_{PR}\cos(N_R-1)a & \vdots \; 0 \\
L_{PR}\sin(a) & \cdots & \cdots & L_{PR}\sin(N_R-1)a & \vdots \; 0 \\
\cdots & \cdots & \cdots & \cdots & \vdots \; \cdots \\
M_{RR}-L_b & M_{RR} & \cdots & M_{RR}-L_b & \vdots \; -L_e/N_R \\
\ddots & \ddots & \ddots & \ddots & \vdots \; \vdots \\
M_{RR}-L_b & L_P & M_{RR}-L_b & M_{RR} & \vdots \; \vdots \\
\ddots & \ddots & \ddots & \ddots & \vdots \; \vdots \\
M_{RR} & \cdots & M_{RR}-L_b & L_P & \vdots \; -L_e/N_R \\
\cdots & \cdots & \cdots & \cdots & \vdots \; \cdots \\
\cdots & \cdots & \cdots & -L_e/N_R & \vdots \; L_e
\end{array}
$$

with: $T_1 = \sqrt{\frac{3}{2}}\,\omega_R M_{SR}$, $L_P = L_{R_p}+2L_b+2\frac{L_e}{N_R}$, $L_{PR} = \sqrt{\frac{3}{2}}\,L_{SR}$. The mechanical equation is:

$$
\frac{\mathrm{d}}{\mathrm{d}t}\omega_m = \frac{1}{J_m}\big(C_e - C_r\big) \tag{16}
$$

where: $\omega_m = \frac{\mathrm{d}\theta_m}{\mathrm{d}t}$ and

$$
C_e = \sqrt{\frac{3}{2}}\,p M_{SR}\Big\{ I_{qS}\sum_{k=0}^{N_R-1} I_{k+1}\cos(ka) \\
- I_{dS}\sum_{k=0}^{N_R-1} I_{k+1}\sin(ka) \Big\}.
$$

4 INCIPIENT ROTOR FAULTS SIMULATION

For a three phase squirrel cage motor with NR-bars, plus one end ring current, equations (15) and (16) can be resolved using the fourth Runge-Kutta method.

Using a computer program written in Matlab, the partial or the total breakage fault in the bar is modelled by the assumed linear change of the value of the resistance R_{bF} named fault bar resistance. The variation of the resistance R_{bF} as a function of time is modelled by relation (17) represented for three cases of the resistance time ratio named α.

$$
R_{bFk} = R_b\big(1 + \alpha(t - t_0)\big) \tag{17}
$$

where: $\alpha = \mathrm{tg}(\gamma)$; angle resistance rate as shown in Fig. 4.
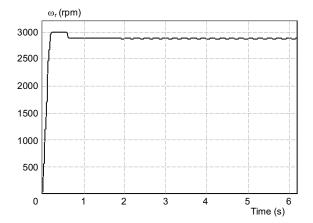
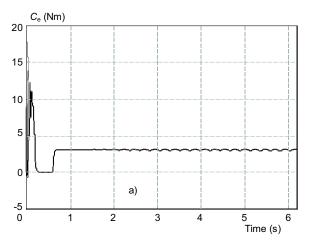**Fig. 5a.** Electrical speed for the healthy motor and broken rotor bar No 2

Fig. 5b. Zoom for the electrical speed for the healthy motor and broken rotor bar No 2

Fig. 6a. Torque for healthy motor and broken bar No 2

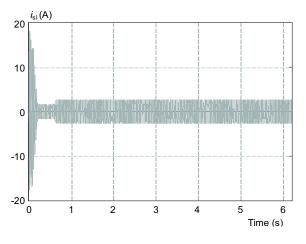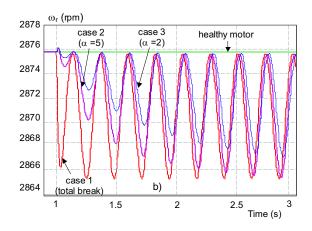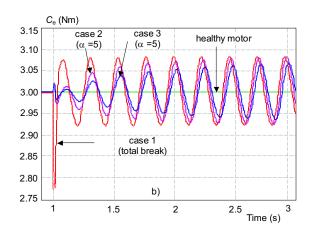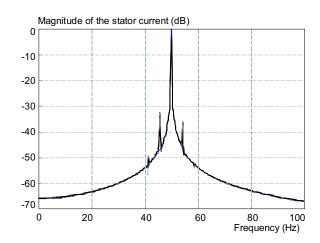**Fig. 6b.** Zoom for the torque cases healthy motor and broken rotor bar No 2

Fig. 7. Stator current of phase 1

Fig. 8. Logarithmic FFT for the stator current from healthy motor and one broken bar No 2

The first case assumes that the broken bar is totally broken at $t_0 = 1$ s. The second one illustrates the medium cases when the partial broken bar time evolution is done by $\alpha = 5$. The third case characterizes the slowly broken bar situation with $\alpha = 2$. The R_{bF}-time evolution is shown in Fig. 4.
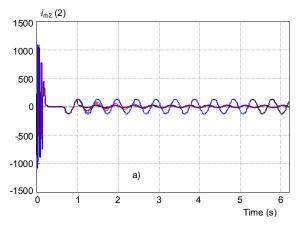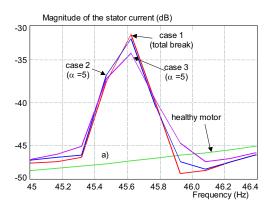
Fig. 9a. Rotor current with broken bar No 2

Fig. 9b. Zoom of the rotor current with broken bar No 2

Fig. 10a. Zoom of the lower frequency

Fig. 10b. Zoom of the upper frequency

The fault is considered in the kth bar and the fault matrix $[R_F]$ is added to the rotor sub-matrix:

$$[R_F] = \begin{bmatrix} 0 & \cdots & 0 & \cdots & \cdots & 0 \\ \vdots & \cdots & \vdots & \vdots & \cdots & \vdots \\ \vdots & \cdots & 0 & 0 & \cdots & 0 \\ 0 & 0 & R_{bF_k} & -R_{bF_k} & 0 & 0 \\ 0 & 0 & -R_{bF_k} & R_{bF_k} & 0 & 0 \\ \vdots & \vdots & 0 & 0 & \vdots & \vdots \\ \vdots & \vdots & \vdots & \vdots & \vdots & \vdots \end{bmatrix}$$

The curves of speed, electromagnetic torque, currents stator and rotor versus time are plotted with applied constant load at 0.6 s. It is considered that the failure of a bar starts at the moment $t_0 = 1$ s as shown in Figs. 5, 6, 7 and 8, respectively.

The oscillations of the curves in Figs. 5b and 6b justify the presence of a break rotor bar defect in the machine.

The oscillations of the current in the fissured bar follow a deadened pattern because the partial break tends towards a total break (Fig. 5b).
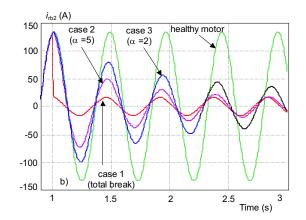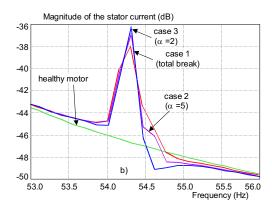
Direct analysis of the stator current, as presented in Fig. 7, does not clearly reveal the presence of the defect because of the weak modulation of the sinusoidal current in the permanent mode.

The appearance of lines at frequencies $(1 \pm 2g)g$ on the spectrum stator current in the permanent mode is highlighted by fast Fourier transform FFT presented in Fig. 8.

Figures 9a and 9b present, respectively, the real rotor bar current versus time. We can observe the broken bar evolution for the three above cases.

Figures 10a and 10b present the zooming of spectrum given by Fig. 8 around the lower and the upper frequency. We can note that the failure detected rotor bar is increased corresponding to the nature of broken bar time evolution. Tables 1, 2 and 3 summarize the evolution of the current spectrum analysis concerning the upper and the lower incipient rotor bar faults taken respectively for three time intervals 1–2 s, 2–3 s and 3–4 s. Through theses tables, we can note the clear increase of the dB-magnitude corresponding to a lower spectrum fault frequency. A reverse situation is also observed from the upper spectrum

fault frequency. Both of the above spectrum fault frequency evolutions indicate the fault presence in the rotor bar since its existence.

Table 1. Current spectrum analysis taken between 1 and 2 seconds after incipient fault

	$\alpha \to \infty$ (case 1)	$\alpha = 5$ (case 2)	$\alpha = 2$ (case 3)
$f_1 = (1-2g)fs$ (Hz)	45.6347	45.6963	45.7349
f'_1 (Hz)	44.5622	44.5552	44.5552
$f_2 = (1+2g)fs$ (Hz)	54.3653	54.3037	54.2651
f'_2 (Hz)	54.3137	54.3265	54.3137
A_1 (dB)	−26.594	−27.193	−27.493
A_2 (dB)	−23.153	−23.483	−23.903

Table 2. Current spectrum analysis taken between 2 and 3 seconds after incipient fault

	$\alpha \to \infty$ (case 1)	$\alpha = 5$ (case 2)	$\alpha = 2$ (case 3)
$f_1 = (1-2g)fs$ (Hz)	45.6347	45.6963	45.7349
f'_1 (Hz)	45.1613	45.1613	45.1613
$f_2 = (1+2g)fs$ (Hz)	54.3653	54.3037	54.2651
f'_2 (Hz)	53.7113	53.7113	53.7113
A_1 (dB)	−23.5973	−23.597	−24.266
A_2 (dB)	−23.175	−22.784	−22.661

f'_1 and f'_2 are deduced using the maximum values of the curves (Fig. 10a) and (Fig. 10b) respectively.

The frequencies calculated according to the relation and deduced from the figures (10a, 10b) show good agreement as indicated in Tables 1, 2 and 3.

In the case of failure of a bar, the distribution of the RMS values currents bars also shows the nature of this failure (partial or total break), as shown in figures 11a, b, c, d.

Table 3. Current spectrum analysis taken between 3 and 4 seconds after incipient fault

	$\alpha \to \infty$ (case 1)	$\alpha = 5$ (case 2)	$\alpha = 2$ (case 3)
$f_1 = (1-2g)fs$ (Hz)	45.6347	45.6963	45.7349
f'_1 (Hz)	45.7691	45.7691	45.7691
$f_2 = (1+2g)fs$ (Hz)	54.3653	54.3037	54.2651
f'_2 (Hz)	54.9329	54.9297	54.9329
A_1 (dB)	−23.488	−22.709	−22.413
A_2 (dB)	−24.549	−24.765	−25.391

5 CONCLUSION

This paper has presented a computer simulation of an incipient rotor bar fault of an induction motor for diagnostic purposes. Based on the developed mathematical model, the computer simulation takes in consideration the influence of the resistance broken bar time evolution.

The spectrum analysis of the stator current shows only the presence of a break of the bar in time evolution (partial or total break). This can be set in obviousness by the analysis of the response of the speed or torque. Indeed, these oscillations increase with the break of the rotor bar. In all cases we can observe incipient oscillations on the speed, torque end stator current. These oscillations will be increased when the bar fissure increases, because the distribution of the rotor bar currents becomes unbalanced.

Nomenclature

l, p Length of the rotor and number of poles pairs respectively.

N_R Number of rotor bars.

N_S Number of effective series connected coils per stator phase.

δ, D Air-gap length and air-gap mean diameter respectively.

R_e Resistance of end ring segment between two adjacent rotor bars.

R_S Resistance of stator phase a winding.

B, α Magnetic flux density and resistance time ratio respectively.

R_b, R_e Rotor bar and rotor ring resistance.

L_b Leakage inductance of rotor bar.

L_e Leakage inductance of end ring segment between two adjacent rotor bars.

L_{Sp} Principal inductance magnetizing stator phase.

L_S, L_{Sf} Total inductance of a stator phase and Leakage inductance respectively.

μ_0, g Permeability of air gap space and slip respectively.

C_e, C_r Electromagnetic torque and torque of load respectively.

ω_r, ω_m Electric and mechanical angular velocity respectively.

I_{Sn} Phases stator currents; $n = 1, 2, 3$ (phase number).

f_S, J_m Stator supply frequency and inertia respectively.

f_1, f_2 Lower and upper frequency respectively of current spectrum.

A_1 Current amplitude at the lower frequency of current spectrum.

A_2 Current amplitude at the upper frequency of current spectrum.

t_0 Moment of the incipient failure.

mmf Magneto-motoric force.

i_{Rk}, i_{bk} Mesh and branch current respectively.

I_e End ring current.
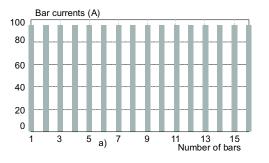
I_{ds}, I_{qs} Direct and quadratic park current.

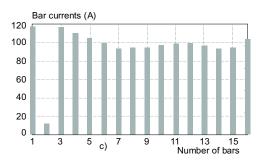**Fig. 11a.** RMS values of the bar currents, healthy motor at $t = 2.5$ s

Fig. 11b. RMS values of the bar currents, one broken bar at $t = 2.5$ s (case 1: $\alpha \to \infty$)

Fig. 11c. RMS values of the bar currents, one partially broken bar at $t = 2.5$ s (case 2: $\alpha = 5$)

Fig. 11d. RMS values of the bar currents, one partially broken bar at $t = 2.5$ s (case 3: $\alpha = 2$)

Appendix

Parameters	Rated Values	Unit
Output power	1.1	(kW)
Stator voltage	220/380	(V)
Stator frequency	50	(Hz)
Pole number	2	
Stator resistance	7.58	(ω)
Rotor resistance	6.3	(ω)
Rotor inductance	0.4612	(H)
Rotor bar resistance	71.5	$(\mu\omega)$
Friction coefficient	0.000	(SI)
Rotor bar inductance	0.1	(μH)
Resistance of end ring segment	1.5	$(\mu\omega)$
Leakage inductance of end ring	0.1	(μH)
Mutual inductance	26.5	(mH)
Length of the rotor	65	(mm)
Air-gap mean diameter	1.5	(mm)
Number of rotor bars	16	
Number of turns per stator phase	160	
Inertia	0.0054	(Kgm^2)

References

[1] YUEN CHOW, MO.: Guest Editorial Special Section on Motor Fault Detection and Diagnosis jour IEEE Transactions on Industrial Electronics.

[2] THOMSON, W. T.—RANKIN, D.: Case Histories of On-Line Rotor Cage Fault Diagnosis, Condition Monitoring Conferences Proceeding, Swansea, 1987, pp. 789–819.

[3] CHOW, T. W. S.—FEL, G.: Three Phase Induction Machine Asymmetrical Faults Identification Using Bispectrum, IEEE Transactions on Energy Conversion **10** No. 4 (1992), 88–93.
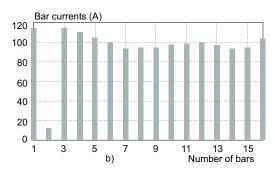
[4] INNES, A. G.—LANGMAN, R. A.: The Detection of Broken Bars in Variable Speed Induction Motor Drives, International Conferences on Electrical Machines, 1994.

[5] SCHOEN, R. R.—HABETLER, T. G.: Effects of Time-Varying Loads on Rotor Fault Detection in Induction Machines, IEEE Transactions on Industry Applications **31** No. 4 (1995), 900–906.

[6] WALLISER, R. F.—LANDY, C. F.: Determination of Interbar Currents in the Detection of Broken Bars in Squirrel Cage Induction Motors, IEEE Transaction on Energy Conversion **9** No. 1 (1994), 152–158.

[7] CAMERON, J. R.—THOMSON, W. T.—DOW, A. B.: One Line Current Monitoring of Induction Motors a Method for Calculating the Level of Air Gap Eccentricity, IEE Conferences on Electrical Machines and Drives, 1987, 173–177.

[8] PENMAN, J.—SEDDING, H. G.—LLOYD, B. A.—FINK, W. T.: Detection and Location of Inter Turn Short Circuits in the Stator Winding of Operating Motors, IEEE Winter Power Meeting, February 1994.

[9] PHEMISTER, T. G.—GREGORGY, G.: Monitoring Fractional Shorted Turns on Generator Rotors, International Conference on Electrical Machines, 1992.

[10] EDERMAN, J.—KERKMAN, R. J.—SCHLEGEL, D.—SKIBINSKI, G.: Effect of PWM Inverters on AC Motor Bearing Currents and Shaft Voltages, APEC'95, 1995, 24–28.

[11] SCHOEN, R. R.—HABETLER, T. G.—KAMRAN, F.—BATHELD, R. G.: Motor Bearing Damage Detection Using Stator Currents Monitoring, IEEE Transaction on Industry Applications **31** No. 6 (1995), 1274–1279.

[12] LIPO, A. R. T. A.: Complex Vector Model of the Squirrel-Cage Induction Machine Including Instantaneous Rotor bar Currents, IEEE Transaction on Industry Application **35** No. 6 (1999).

[13] NOVOTNY, D. W.—LIPO, T. A.: Vector Control and Dynamics of AC Drives, Clarendon Press, Oxford, 1996.

[14] VIEIRA, M.: Estimation bayèsienne par des méthodes MCMC Application à la surveillance des moteurs asynchrones, Thèse doctorat Science pour ingénieur, Université de Nice, 25 Janvier 1999.

Menacer Arezki was born in Batna, Algeria, in 1968. He received the BSc degree in Electrical Engineering, from the University of Batna, Algeria, in 1992, and the MSc degree in Electrical and Computer Engineering from Electrical Engineering Institute of Biskra University, Algeria, in 1996, Since graduation, he has been with the University of Biskra, Algeria, where he is a Teaching Assistant at the Electrical Engineering Institute. He is the member of the Research Laboratory of Electromagnetic Induction and Propulsion Systems of Batna, Algeria and Research Laboratory of Electrotechnic of Biskra, Algeria. He is currently working on his PhD dissertation on the electric machines and drives control and diagnosis at the University of Batna, Algeria.

Mohamed-Said Nait-Said was born in Batna, Algeria, in 1958. He received the BSc degree in Electrical Engineering from the National Polytechnic Institute of Algiers, Algeria, in 1983, and the MSc degree in Electrical and Computer Engineering from Electrical Engineering Institute of Constantine University, Algeria, in 1992,. He received the PhD degree in Electrical and Computer Engineering from University of Batna, in 1999. Currently, he is an Associate professor at the Electrical Engineering Institute at the University of Batna. He is the head of the Research Laboratory of Electromagnetic Induction and Propulsion Systems of Batna. His is also research interests include electric machines and drives control and diagnosis.

Said Drid was born in Batna, Algeria, in 1969. He received the BSc degree in Electrical Engineering, from the University of Batna, Algeria, in 1994, and the MSc degree in Electrical and Computer Engineering from Electrical Engineering Institute of Batna University, Algeria, in 2000, Since graduation, he has been with the University of Batna, Algeria, where he is a Teaching Assistant at the Electrical Engineering Institute. He is the member of the Research Laboratory of Electromagnetic Induction and Propulsion Systems of Batna, Algeria. He is currently working on his PhD dissertation on the control of induction motors at the University of Batna, Algeria.

Benakcha A/Hamid was born in 1961 in Arris, Algeria. He had a MSc in 1980, a BSc in 1983 from the University of Batna, Algeria, a Master of Science in 1985 and a PhD in electronics from the University of Clermont-Ferrand, France. Since 1991, he teaches at the University of Biskra, Algeria. He is the member of the Research Laboratory of electrotechnic of Biskra and the head of the research group "Simulation of sliding mode control of an asynchronous machine". His other research interests are: Electric machines (design, modelling, identification, control), power electronics, electromagnetism (antennas, free propagation), electronics (television).